NASA/TM–20250004554

A Transmission Line Impedance Prediction Model for Acoustic Liners

Michael G. Jones, Douglas M. Nark, and Jordan R. Kreitzman
Langley Research Center, Hampton, Virginia

August 2025

NASA STI Program Report Series

Since its founding, NASA has been dedicated to the advancement of aeronautics and space science. The NASA scientific and technical information (STI) program plays a key part in helping NASA maintain this important role.

The NASA STI Program operates under the auspices of the Agency Chief Information Officer. It collects, organizes, provides for archiving, and disseminates NASA's STI. The NASA STI Program provides access to the NTRS Registered and its public interface, the NASA Technical Report Server, thus providing one of the largest collections of aeronautical and space science STI in the world. Results are published in both non-NASA channels and by NASA in the NASA STI Report Series, which includes the following report types:

- TECHNICAL PUBLICATION. Reports of completed research or a major significant phase of research that present the results of NASA programs and include extensive data or theoretical analysis. Includes compilations of significant scientific and technical data and information deemed to be of continuing reference value. NASA counterpart of peer-reviewed formal professional papers, but having less stringent limitations on manuscript length and extent of graphic presentations.
- TECHNICAL MEMORANDUM. Scientific and technical findings that are preliminary or of specialized interest, e.g., quick release reports, working papers, and bibliographies that contain minimal annotation. Does not contain extensive analysis.
- CONTRACTOR REPORT. Scientific and technical findings by NASA-sponsored contractors and grantees.
- CONFERENCE PUBLICATION. Collected papers from scientific and technical conferences, symposia, seminars, or other meetings sponsored or co-sponsored by NASA.
- SPECIAL PUBLICATION. Scientific, technical, or historical information from NASA programs, projects, and missions, often concerned with subjects having substantial public interest.
- TECHNICAL TRANSLATION. English- language translations of foreign scientific and technical material pertinent to NASA's mission.

Specialized services also include organizing and publishing research results, distributing specialized research announcements and feeds, providing information desk and personal search support, and enabling data exchange services.

For more information about the NASA STI Program, see the following:

- Access the NASA STI program home page at `http://www.sti.nasa.gov`
- Help desk contact information: `https://www.sti.nasa.gov/sti-contact-form/` and select the "General" help request type.

NASA/TM–20250004554

A Transmission Line Impedance Prediction Model for Acoustic Liners

Michael G. Jones, Douglas M. Nark, and Jordan R. Kreitzman
Langley Research Center, Hampton, Virginia

National Aeronautics and
Space Administration

Langley Research Center
Hampton, Virginia 23681-2199

August 2025

Acknowledgments

This work was conducted in support of the Advanced Air Transport Technology Project of the NASA Advanced Air Vehicles Program.

Available from:

NASA STI Program / Mail Stop 150
NASA Langley Research Center
Hampton, VA 23681-2199

Abstract

A Zwikker and Kosten Transmission Line model is used to predict the acoustic impedance at the surface of an acoustic liner. Multiple versions of this model, labeled as ZKTL, have been used at the NASA Langley Research Center for five decades. The latest version (titled ZKTL-SC) is presented, including descriptions of component models to compute sound transmission through different types of layers that might constitute an acoustic liner. This model computes the sound transmission from the backplate to the surface of a single chamber of the liner. Results for multiple chambers can then be combined to compute an effective (smeared) impedance over their combined surfaces. Multiple updates are included in this version. A "single channel" model considers the physics of individual chambers that comprise the entire acoustic liner. This allows a more unified modeling approach to be applied. An updated model is used to account for the effects of thick partitions between adjacent liner chambers, a feature that has become more prevalent with the advent of additively manufactured liners. Implementation of chambers filled with bulk material has also been updated to use a similar modeling approach to that employed with local-reacting liners. Finally, experimental results have been compiled to support validation of each of the models used for the variety of chamber types considered.

Nomenclature

Symbols	**Description**
A_s, A_c, A_p	cross-sectional area of liner surface, active chamber, and individual perforate
c, C_D, σ	sound speed, discharge coefficient, and open area ratio
d, D	hole diameter, and chamber equivalent diameter
f, k, ω	frequency, freespace wavenumber ($= \omega/c$), and angular frequency
h, j	height of layer and imaginary unit $\left(= \sqrt{-1}\right)$
J_0, J_2	Bessel functions of first kind with orders 0 and 2
M_{ave}	average Mach number
N_c, N_p	number of chambers and perforations
p_n, u_n	acoustic pressure and particle velocity at vertical location n
P_n, P_{ref}	Prandtl number and reference pressure ($20\,\mu$Pa)
R_f, R_1	flow resistance and flow resistivity
s, u_{RMS}	shear wavenumber and RMS acoustic particle velocity
ϵ, n_Γ	intermediate calculations for perforate model
$T_{11}, T_{12}, T_{21}, T_{22}$	transmission matrix coefficients
Γ, ζ_c	characteristic impedance and propagation constant
$\lambda, \gamma, \delta_1$	wavelength, specific heat ratio, and boundary layer displacement thickness
β, β_{bp}	normalized acoustic admittance of liner and backplate
$\zeta_s, \zeta_{\text{ch}}$	acoustic impedance at surface of liner and individual chamber
ζ_{MKM}	impedance predicted with Motsinger and Kraft Modified model
$\theta, \chi, \zeta_{\text{tran}}$	normalized resistance and reactance, and transfer impedance
ρ, μ	density and viscosity of air

Abbreviations	**Description**
NIT	Normal Incidence Tube
MKM	Motsinger and Kraft Model
RMS	root mean squared
SDOF	single degree of freedom
SPL	sound pressure level
ZKTL	transmission line model based on the Zwikker and Kosten formulation
ZKTL-SC	single chamber version of the ZKTL model

1 Introduction

Although much progress in noise reduction has been made over the last 50 years, the level of noise radiated from commercial aircraft to the communities surrounding airports remains significant. Acoustic liners mounted in the walls of the aircraft engine nacelle are used to reduce noise due to the rotating fan and associated mechanics. The NASA Langley Liner Physics Team continues to work in multiple areas to support the implementation of optimally designed acoustic liners. This includes (1) implementation of improved measurement and data analysis tools for evaluation of the acoustic and aerodynamic performance of liners (e.g., impedance eduction and liner drag measurement), (2) modeling and assessment of novel liner configurations, and (3) development of propagation codes to predict the attenuation achievable via acoustic liners.

The NASA team has used a number of impedance prediction models over the last 40 years. Much attention has been given to perforate facesheet models [1] and a transmission line model titled ZKTL [2]. This paper provides a description of a recent version of the ZKTL model, labeled as ZKTL-SC, that focuses on computation for a single chamber of a liner.

Previous versions of the ZKTL model were designed to predict the surface impedance of an entire acoustic liner, assumed to be comprised of multiple chambers. Each of these chambers were allowed to contain different configurations. As a result, the multi-channel versions became somewhat unwieldy (too many options to support a unified modeling approach). The current version employs a unified approach to modeling each of the types of chambers, including a liner chamber filled with bulk material. With the advent of additively manufactured liners, the effects of partition thickness have become more important. Earlier models were focused on conventional acoustic liners, for which the partition thickness has typically been negligible. However, the additive manufacturing process currently requires the partitions to be sufficiently thick as to have a more significant effect on the liner impedance.

Multilayer acoustic liners can be modeled using this transmission line approach, in which the change in acoustic pressure and normal particle velocity across each layer is used to determine the resultant values for these two parameters at the surface of the liner. The specific acoustic impedance is then computed as the ratio of the acoustic pressure to the acoustic particle velocity at the surface of the liner. Figure 1 presents a sketch of a notional 10-layer liner with two identical chambers. This design is presented to draw attention to the fact that the ZKTL-SC model is capable of combining the effects of a variety of layers into a single chamber acoustic impedance computation. The odd-numbered layers are open-air pathways. Layer 2 can be viewed as a very thick perforate sheet, while Layers 4 and 10 represent perforate sheets with more conventional dimensions (i.e., where the hole and sheet thicknesses are nominally the same). Layer 6 represents a wire mesh septum (sometimes also used as a facesheet) and Layer 8 depicts a porous material (e.g., foam).

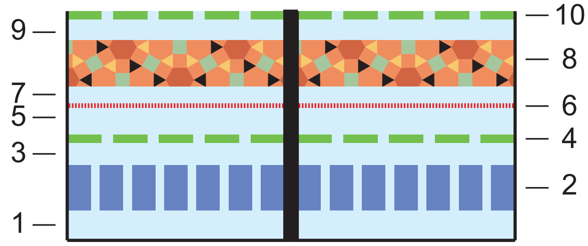

Figure 1: Sketch of two chambers of a 10-layer liner.

The remainder of this paper is organized as follows. Section 2 presents an overview of the transmission line modeling approach, and Section 3 provides a brief review of the transmission matrices used to model each of the layer types. A brief description of the NASA Normal Incidence Tube (NIT) is provided in Section 4, and a comparison of predicted and measured results is presented in Section 5. Finally, concluding remarks are captured in Section 6.

2 Analysis Overview

This section provides an overview of the transmission line model used to describe the acoustic performance of local-reaction acoustic liners[1]. A description of a single active chamber is provided. The effects of combining multiple chambers are then discussed, first with negligible partitions such as those present in typical aircraft engine nacelle liners, and then with thicker partitions generally required for additively-manufactured liners.

Note that all impedances used in this paper are normalized by ρc, the characteristic impedance of air. A corresponding normalization of admittances is also assumed. The acoustic pressure and acoustic particle velocity are normalized by ρc^2 and c, respectively. Finally, an $e^{j\omega t}$ time convention is assumed.

2.1 Single Chamber

A single active chamber of an acoustic liner (e.g., the left side of Fig. 1) is the basic component of this analysis. In this usage, the term 'active' is used to denote that portion of the chamber that does not include the partitions between chambers. The analysis starts by defining the normalized acoustic pressure and particle velocity at the surface of the backplate (vertical location 0) as

$$\begin{pmatrix} p_0 \\ u_0 \end{pmatrix} = \begin{pmatrix} 1 \\ \beta_{\text{bp}} \end{pmatrix}, \tag{1}$$

where β_{bp} is the acoustic admittance (inverse of the acoustic impedance) at the surface of the backplate. This admittance is zero (frequency-independent) for a rigid backplate. At each successive

[1]Local-reaction acoustic liners typically contain partitions that inhibit sound transfer through the body of the liner, such that the sound absorption is spatially concentrated.

transition (i.e., across a layer or across an interface into or out of a layer, depending on the type of layer), a transmission matrix equation

$$\begin{pmatrix} p_{n+1} \\ u_{n+1} \end{pmatrix} = \begin{pmatrix} T_{11} & T_{12} \\ T_{21} & T_{22} \end{pmatrix} \begin{pmatrix} p_n \\ u_n \end{pmatrix} \quad (2)$$

is used to compute the change in acoustic pressure and particle velocity. The models used to define the transmission matrices for a number of layer types are provided in Section 3.

2.2 Multichamber Effects

Typical acoustic liners consist of multiple chambers, so a method to properly compute the combined effects of multiple chambers is presented. When the partitions that separate these adjacent chambers become sufficiently thick, they can impact the acoustic impedance that is present at the liner surface. An approach to incorporate these effects into the computation of the liner impedance is also provided.

2.2.1 Uniform-impedance liners

Local-reaction liners typically contain multiple chambers. The most common configuration is for these liners to be uniform, i.e., each chamber is identical to all other chambers in the liner. For uniform liners with negligible partition thickness (e.g., SDOF liner with conventional phenolic honeycomb core), the surface impedance is identical to that computed at the surface of the individual active chamber. This impedance is given by the ratio of the acoustic pressure to acoustic particle velocity computed at the surface of the individual chamber, regardless of the number of layers used to construct the chamber or the number of chambers that make up the liner.

2.2.2 Variable-impedance liners

One method to increase the frequency bandwidth of sound absorption is to group multiple SDOF chambers together such that each chamber (or subgroup of chambers) is tuned to a different frequency via a different chamber height (see Fig. 2). This is typically labeled as a variable-depth liner. In a more general sense, it should be noted that any method of varying the impedance with distinct local-reaction liner configurations (e.g., see Fig. 3) can be used to achieve broadband sound absorption.

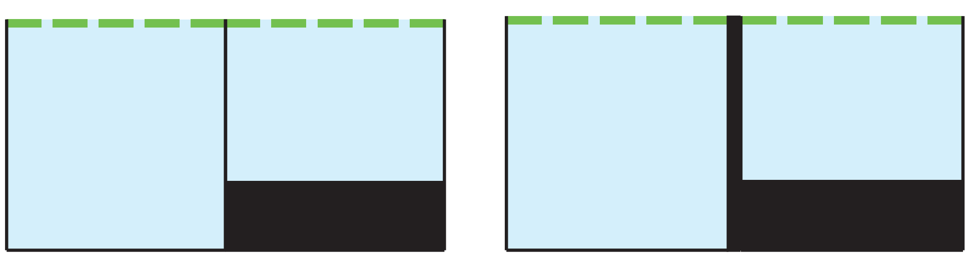

(a) Negligible partition thickness. (b) Thick partition.

Figure 2: Sketch of variable-depth liners with negligible and thick partitions.

The surface impedance of the entire liner is given by

$$\zeta_s = \left(\frac{1}{A_s} \sum_{i=1}^{N_c} \frac{A_{c,i}}{\zeta_{c,i}} \right)^{-1} \tag{3}$$

when the following conditions are met:

1. The impedances at the surfaces of each active chamber, $\zeta_{c,i}$, are known.
2. The combined cross-sectional sizes of these surfaces are confined to a spatial extent of less than $\lambda/3$ at the highest frequency of interest [3].
3. The partitions that separate the chambers have negligible thickness (e.g., conventional phenolic honeycomb core, see Figs. 2a and 3).

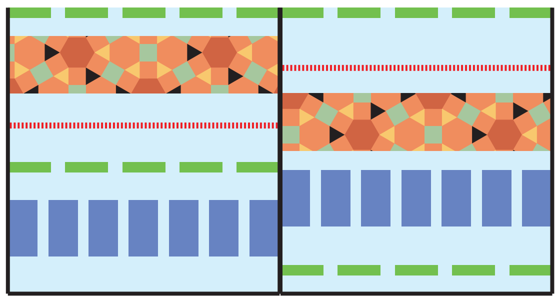

Figure 3: Sketch of variable-impedance liner with negligible partitions.

2.2.3 Partition thickness

The modeling approach described above is appropriate for conventional aircraft honeycomb material for which the partition thickness is negligible (for our purposes, thicknesses of up to 0.010" are considered negligible). However, additively-manufactured samples often require partitions with increased thickness, such as the thick partition that separates the two chambers in Figs. 1 and 2b.

Partition thickness effects were addressed in an earlier report [4] for two types of liner facesheets: wire mesh and perforated plate. In that report, the transfer impedance across the facesheet was treated as an independent process from the computation of the impedance at the surface of the core. This was simple for a wire mesh facesheet, where the transition impedance due to the addition of the wire mesh was simply the application of a lumped-element model that increased the acoustic pressure by an amount corresponding to the normalized flow resistance of the mesh. For the perforated sheet, the Motsinger and Kraft impedance prediction model [5] was applied. This approach attempted to include the partitions as an intrinsic part of the computation.

In contrast, the current approach accounts for a perforate facesheet via a lumped-element model that can be directly included within the transmission matrix, such that the results remain confined to the active chamber. In this approach, the solid partition is simply treated as an additional 'chamber' in Eq. [3]. The impedance is assumed to be infinite (i.e., $\beta = 0$) for this portion of the surface. Since the current approach integrates the effects of the facesheet directly into the transmission line computation, it is simpler to implement and therefore is the preferred choice of the authors.

3 Transmission Matrices for Different Layer Types

Three approaches are considered for computation of sound transmission across a single layer. In the first approach, sound is assumed to propagate through the layer, thereby enabling determination of the change in acoustic pressure and velocity (and hence, acoustic impedance) across the layer. In the second, the layer is assumed to be sufficiently thin such that a lumped-element approach may be used to account for changes in acoustic pressure across the layer (velocity is unchanged). The third approach combines acoustic propagation through individual openings with changes in acoustic velocity caused by the sound entering and exiting those openings.

3.1 Acoustic propagation option

When the propagation constant, Γ, and characteristic impedance, ζ_c, are known, the sound propagation can be computed across the layer using equations provided by Zwikker and Kosten [6]. The current impedance prediction model uses this approach for layers comprised of air or porous material.

3.1.1 Open-air layer

The first layer type is comprised of an air gap with height h, as depicted in Fig. 1 via layers 1, 3, 5, 7, and 9. An enlarged view of an open-air layer is provided in Fig. 4, where ports n and $n+1$ are the inlet and outlet, respectively, of the layer. For this type of layer, Γ and ζ_c are computed from Zwikker and Kosten's models (as presented by Tijdeman [7]) via

$$\Gamma = \sqrt{\frac{J_0(j^{3/2}s)}{J_2(j^{3/2}s)}}\sqrt{\frac{\gamma}{n_\Gamma}} \quad \text{and} \quad \zeta_c = \frac{-i}{\Gamma}\frac{J_0(j^{3/2}s)}{J_2(j^{3/2}s)}, \tag{4}$$

where

$$n_\Gamma = \left[1 + \frac{\gamma - 1}{\gamma}\frac{J_2(j^{3/2}P_n^{1/2}s)}{J_0(j^{3/2}P_n^{1/2}s)}\right]^{-1} \quad \text{and} \quad s = \frac{D}{2}\sqrt{\frac{\rho\omega}{\mu}}. \tag{5}$$

Equation [2] is used to compute the transition from (p_n, u_n) to (p_{n+1}, u_{n+1}), where the transmission matrix is given by

$$\begin{pmatrix} T_{11} & T_{12} \\ T_{21} & T_{22} \end{pmatrix} = \begin{pmatrix} \cosh(k\Gamma h) & \zeta_c \sinh(k\Gamma h) \\ \zeta_c^{-1} \sinh(k\Gamma h) & \cosh(k\Gamma h) \end{pmatrix}. \tag{6}$$

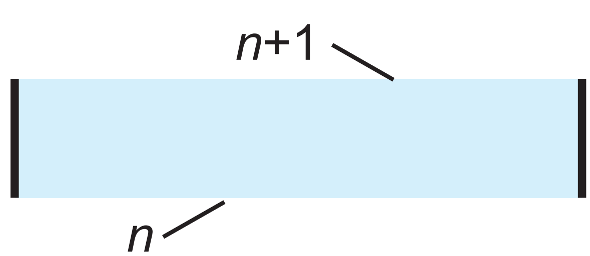

Figure 4: Sketch of open-air pathway layer.

3.1.2 Porous material layer

There are two methods used to determine Γ and ζ_c when the layer is comprised of porous material (Fig. 5).

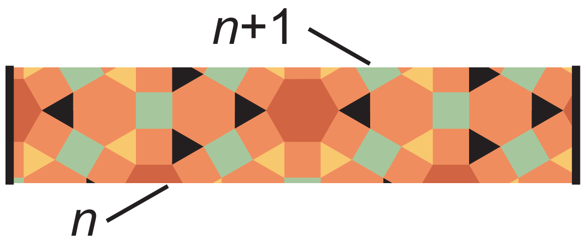

Figure 5: Sketch of porous material layer.

Delany-Bazley-Miki Model

The first method uses the flow resistivity and layer height of a homogeneous porous material as input for equations presented by Delaney and Bazley [8] and later modified by Miki [9] to estimate Γ and ζ_c. These equations are given by

$$\Gamma = \left(0.160\left(\frac{f}{R_1}\right)^{-0.618}\right) + j\left(1 + 0.109\left(\frac{f}{R_1}\right)^{-0.618}\right) \tag{7}$$

and

$$\zeta_c = \left(1 + 0.070\left(\frac{f}{R_1}\right)^{-0.632}\right) - j\left(0.107\left(\frac{f}{R_1}\right)^{-0.632}\right), \tag{8}$$

where

$$R_1 = \frac{R_f}{h}. \tag{9}$$

According to their analysis, this model should give adequate results for conditions where

$$0.01 < f/R_1 < 1.00.$$

Intrinsic properties known

The second method assumes the characteristic impedance and propagation constant have been determined using other means. For example, these parameters can be computed directly using the Johnson-Champoux-Allard-Pride-Lafarge (JCAPL) equations [10–13] if sufficient detail is known regarding the selected porous material.

For materials where this detailed information is not available, the NASA team often employs the Two-Thickness or Two-Cavity Methods [14]. The Two-Thickness Method requires two samples of the material, each with a different thickness, backed with a rigid plate. The Two-Cavity Method requires only one sample, which is tested with two air gap thicknesses between the porous material and the rigid backplate. Each of these configurations can be described via an equation with two unknowns (Γ and ζ_c).[2] Thus, with two measurements of samples at carefully selected thicknesses (either the porous material or the air gap beneath the porous material), the propagation constant and characteristic impedance of the porous material can be determined. Regardless of the method used to determine Γ and ζ_c, sound transmission across the layer of porous material can then be computed using Eqs. [6] and [2].

3.2 Lumped element option

This option is used for layers that are sufficiently thin such that wave propagation through the layer is not supported. In this case, the transmission matrix is given by

$$\begin{pmatrix} T_{11} & T_{12} \\ T_{21} & T_{22} \end{pmatrix} = \begin{pmatrix} 1 & \zeta_{\text{tran}} \\ 0 & 1 \end{pmatrix}, \tag{10}$$

where ζ_{tran} is used to represent the change in impedance across the layer. This is used with Eq. [2] to determine the change in acoustic pressure across the layer.

3.2.1 Resistive layer

Perhaps the most common resistive layer (Fig. 6) is a simple wire mesh. This type of material is often employed as a septum (internal layer) for liners used on the walls of commercial aircraft engine nacelles. It is also sometimes used as a facesheet for the liner.

The transfer impedance for a resistive layer is given by

$$\zeta_{\text{tran}} = \frac{R_f}{\rho c}, \tag{11}$$

where the flow resistance R_f, of the resistive layer is generally determined via measurements conducted with a raylometer [15] (a test rig used to measure the static pressure drop across a material as a function of the mean velocity through the material).

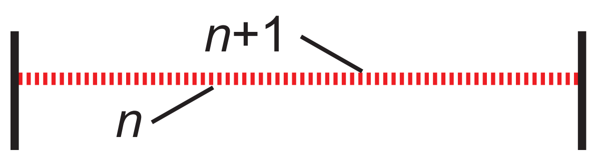

Figure 6: Sketch of resistive layer.

3.2.2 Thin perforated sheet

For conventional perforated sheets where the sheet thickness and hole diameter are nearly the same ($h \approx d$, see Fig. 7), the transfer impedance across the layer can be computed using a perforated facesheet impedance model [1]. The model that is currently applied is a modified version of the Motsinger and Kraft Model given by

[2]Note that the NASA Langley versions of the Two-Thickness and Two-Cavity Methods output a dimensional version of the propagation constant, $G = k\Gamma$.

$$\zeta_{\mathrm{MKM}} = \zeta_{\mathrm{tran}} + \frac{p_n}{u_n} = \frac{32\,\mu h}{\rho c\,(\sigma C_D)\,d^2} + \frac{0.98}{2c\,(\sigma C_D)^2} u_{\mathrm{RMS}} + \frac{M_{\mathrm{ave}}}{\sigma\,\{2 + 3.32\,(\delta_1/d)\}} + j\,\frac{k(h+\epsilon d)}{\sigma} + \frac{p_n}{u_n}, \quad (12)$$

where

$$\epsilon = \frac{0.65\,(1.0 - 0.95\sqrt{\sigma})}{1 + 305\,M_{\mathrm{ave}}^3} \quad (13)$$

and the impedance of the portion of the chamber that is below the perforated sheet is captured via the p_n/u_n term.

The RMS acoustic particle velocity is typically determined via

$$u_{\mathrm{RMS}} = \frac{P_{\mathrm{ref}} 10^{\mathrm{SPL}/20}}{\rho c\,|\zeta_{\mathrm{MKM}}|}. \quad (14)$$

Since this parameter varies with the impedance at the surface of the perforated sheet, ζ_{MKM} and u_{RMS} must be determined iteratively. Equation [12] is then used to separate out the ζ_{tran} term for use in Eq. [10].

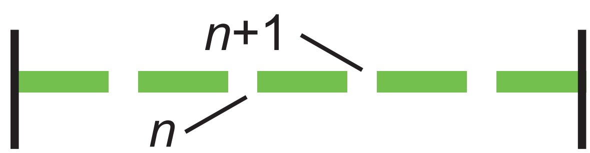

Figure 7: Sketch of thin perforated sheet.

Some of the parameters are computed differently depending on whether the perforated sheet is used as a septum or a facesheet. When the sheet is used as a septum, the proper choice of the SPL will depend on other factors and is therefore left to the user to decide which is best. One option is proposed by Kreitzman and Jones [16], where the backplate acoustic pressure is iterated upon until the target surface SPL is reached. By doing this, appropriate particle velocity effects are captured for every element within the transmission line. Also, there is clearly no contribution due to mean flow ($M_{\mathrm{ave}} = 0$) for the septum. When used as a facesheet, the total SPL at the liner surface is assumed to be known and is therefore used in the computation. Additionally, if tangential mean flow is present at the liner surface, this is included in the computation as well.

3.3 Thick perforated sheet

The last type of layer is a much thicker perforate sheet ($h \gg d$, see Fig. 8). As with the other layer types, the goal of the computation is to determine the change in acoustic pressure and particle velocity (and hence, acoustic impedance) between locations n and $n+1$. However, there are additional transitions that are incorporated into this computation, as depicted in Fig. 9.

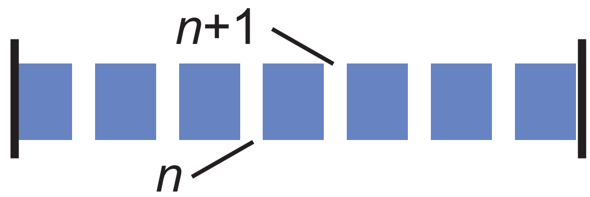

Figure 8: Sketch of thick perforated sheet.

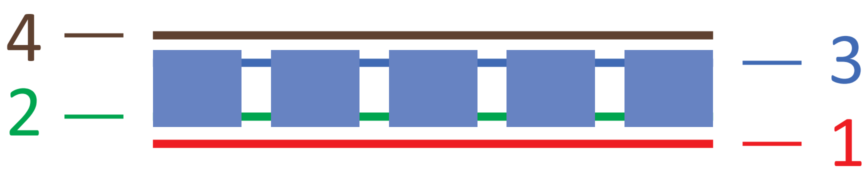

Figure 9: Expanded view of thick perforated sheet.

It is assumed that the acoustic pressure and particle velocity are known at the horizontal plane at vertical location 1 (i.e., equal to the outlet pressure and velocity from the previous layer, corresponding to plane n in Fig. 8). The acoustic pressure and acoustic mass flow are assumed to be constant across the interface between planes 1 and 2. These are, respectively, given by

$$p_2 = p_1 \text{ and } u_2 = \frac{A_c u_1}{N_p A_p}. \tag{15}$$

Sound transmission between planes 2 and 3 is computed as described in Section 3.1.1 with just one difference. For this computation, the shear wavenumber is computed as

$$s = \frac{d}{2}\sqrt{\frac{\rho\omega}{\mu}}, \tag{16}$$

where the chamber diameter D in Eq. [5] is replaced by the hole diameter d. Again, it is assumed that the acoustic pressure and acoustic mass flow are constant across the interface between planes 3 and 4 (corresponds to vertical plane $n+1$ in Fig. 8). These are given by

$$p_4 = p_3 \text{ and } u_4 = \frac{N_p A_p u_3}{A_c}. \tag{17}$$

Note that this layer type is assumed to be linear, whereas the perforate facesheet model used in Section 3.2.2 attempts to account for nonlinear effects via the RMS acoustic particle velocity term. However, this is assumed to be acceptable since nonlinear effects are minimal when $h \gg d$.

4 Normal Incidence Tube (NIT)

The NASA Langley Normal Incidence Tube (Fig. 10a) was used to determine the surface impedance for the test samples considered in this study. This 2”×2”×36” waveguide uses six acoustic drivers to generate a controlled-amplitude, swept-sine source [17]. Three microphones (represented as red dots in Fig. 10b) are flush-mounted with the interior wall of the NIT. One is used as a reference microphone that enables the source magnitude to be set to a desired level, and the other two are mounted in a rotating plug that enables precise interchange of their positions. Acoustic pressures acquired with these microphones are used with the Two-Microphone Method (TMM) [15, 18, 19] to determine the surface acoustic impedance of the test liner. The discussion for each layer type in Section 5 includes a description of the liner configuration and test conditions used in this study.

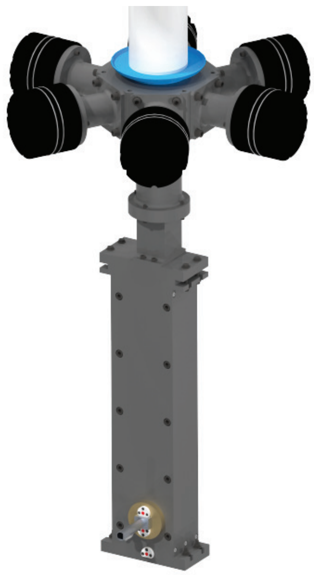

(a) Full NIT.

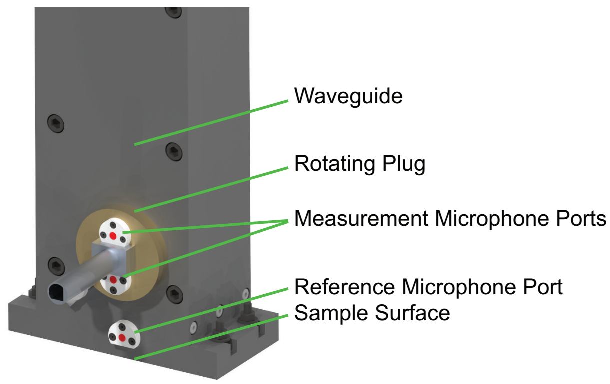

(b) Measurement section expanded view.

Figure 10: Drawings of the NASA Langley Normal Incidence Tube (NIT).

5 Model Validation

Results for sample cases that use each of the layer types are presented in this section. These impedance predictions are compared against impedance spectra educed from data acquired in the NIT. Test samples are chosen from those acquired by the NASA Liner Physics Team in support of a number of other tests. The comparisons included here are intended to demonstrate the features of the ZKTL-SC analysis model, and are not intended to represent the best (or worst) possible comparisons achieved with the underlying models for each layer type. It should be noted that the actual partition thicknesses are included in each validation case presented here using the approach described in Section 2.2.3. Computations for other samples with increased surface blockage appear to confirm the validity of this approach, but will need to be further assessed in future studies.

5.1 Open-Air Layer

Figure 11 presents a comparison of normalized impedance spectra for an open layer such as that depicted in Fig. 4 with the addition of a rigid backplate. The height of the air layer is 1.51" and the chamber is hexagonal (conventional phenolic honeycomb core) with a flat-to-flat surface dimension of 0.375". The source SPL for this test is set to 120 dB.

The viscothermal losses along the chamber walls are expected to be very small for a chamber of this size. The sound field in this chamber is confined to plane waves and the chamber thus behaves as a quarter-wavelength resonator, i.e., the reactance is approximated by $\chi = -j\cot(kh)$. The comparison of the predicted and measured impedance spectra is quite favorable.

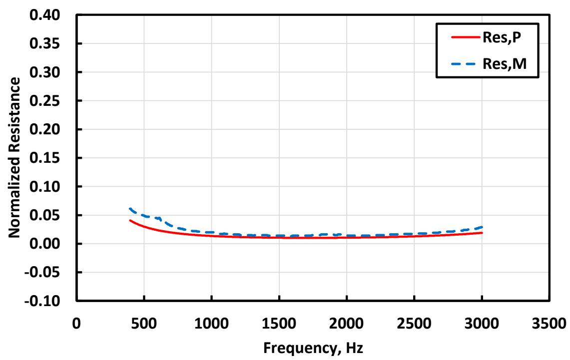

(a) Normalized resistance spectra.

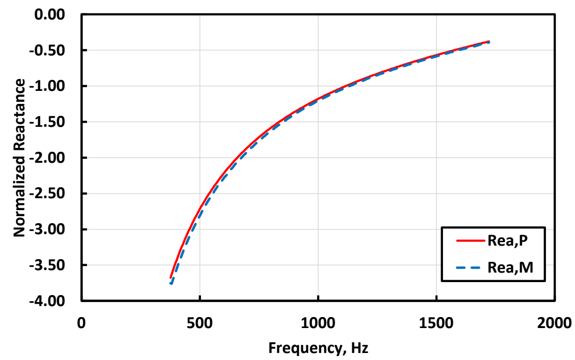

(b) Normalized reactance spectra.

Figure 11: Predicted (P) and measured (M) impedance spectra for an open-air layer with a rigid backplate.

5.2 Porous Material Layer

Two modeling approaches are considered for use with porous material layers. The first is based on a model that uses the flow resistivity to determine the surface impedance of a chamber containing porous material, while the second is based on the Two-Cavity Method, wherein two similar samples with different layer thicknesses are tested and used to infer the bulk properties.

Figure 12 provides results for a 0.5"-thick layer of foam with a flow resistance of 1080 MKS Rayls, backed with a rigid backplate. This foam was selected because it is currently being considered for use in an upcoming acoustic scattering test. The flow resistivity measured in the NASA raylometer [15] is used with the Delany-Bazley-Miki equations (Eqs. [7 - 9]) to predict the surface impedance spectra of the sample. This predicted impedance is compared with experimental data acquired in the NIT with a source SPL of 120 dB. The model slightly underpredicts the measured resistance spectrum but the comparison of predicted and measured reactance spectra is favorable, especially considering the very limited amount of information (DC flow resistance and layer thickness for the bulk material) that is included for this type of analysis. The anomalous behavior in the measured resistance at the lower frequencies is believed to be due to the large reactance magnitude and a corresponding poor sound absorption of the material at those frequencies.

Figures 13 and 14 present results for an additively-manufactured bulk material, for which the Two-Cavity Method [14] was used to determine the frequency-dependent values of the propagation constant and characteristic impedance. This TPMS (triply periodic minimal surface) material was evaluated in a recent investigation by Brown et al. [20], for which the cell structure can be carefully designed to achieve desired acoustic characteristics [20]. The source SPL for each of these tests was 120 dB.

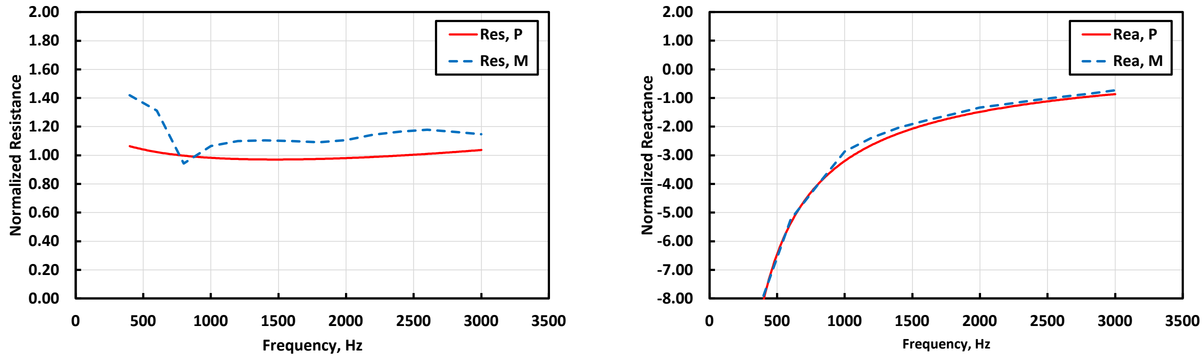

(a) Normalized resistance spectra.

(b) Normalized reactance spectra.

Figure 12: Predicted (P) and measured (M) impedance spectra for a Nomex liner with a rigid backplate, modeled using Delany-Bazley-Miki equations.

Figure 13 compares predicted and measured impedance spectra for a configuration where the porous material is backed with a rigid backplate. Excellent agreement is observed for this 1.5”-thick configuration.

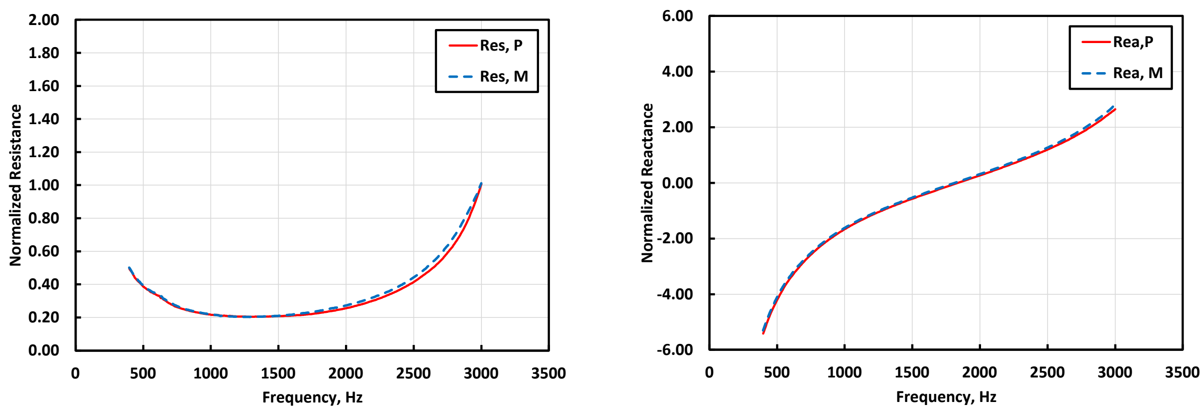

(a) Normalized resistance spectra.

(b) Normalized reactance spectra.

Figure 13: Predicted (P) and measured (M) impedance spectra for a TPMS liner with a rigid backplate, using values of Γ and ζ_c derived from the Two-Cavity Method.

Figure 14 provides the corresponding results for a configuration in which there is a 0.5”-thick air gap between the rigid backplate and the 1.5”-thick porous material. Although there is a slight disagreement between the predicted and measured values for frequencies near antiresonance (frequency where reactance crosses zero with negative slope), the agreement is generally quite good.

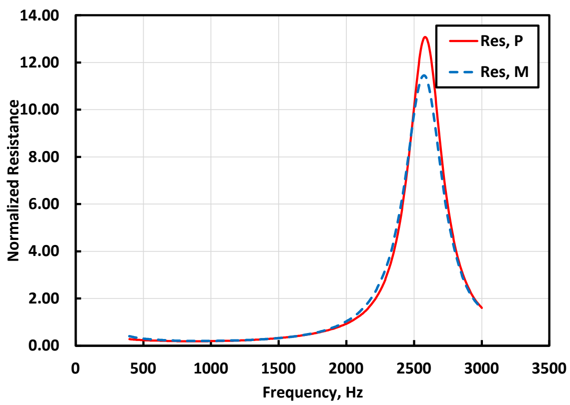

(a) Normalized resistance spectra.

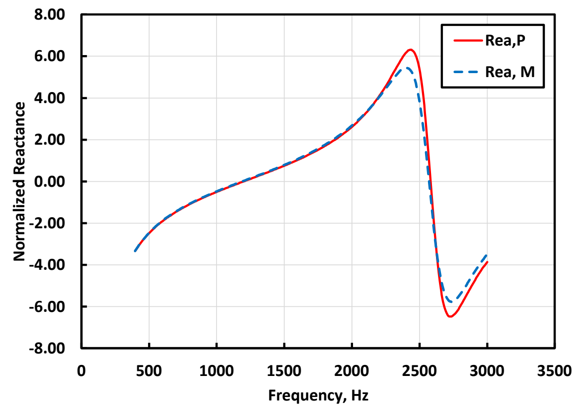

(b) Normalized reactance spectra.

Figure 14: Predicted (P) and measured (M) impedance spectra for a TPMS layer above a 0.5"-thick air gap and a rigid backplate, using values of Γ and ζ_c derived from the Two-Cavity Method.

5.3 Resistive Layer

Figure 15 presents a comparison of normalized impedance spectra for a sample comprised of a 270 MKS Rayls wire mesh over a 1.5"-thick air gap with a rigid backplate. This wire mesh has been used for many NASA tests, as it provides a convenient facesheet material for which the acoustic properties are very weakly nonlinear. This test was conducted with a source SPL of 140 dB. This SPL was chosen to capture any possible nonlinear effects for this liner type. Viscothermal losses along the chamber walls are assumed negligible due to the cross-sectional dimensions of these chambers. As such, the resistance of this liner is typically assumed to be almost entirely driven by the normalized flow resistance of the facesheet, i.e.,

$$\theta \approx \frac{R_f}{\rho c} = \frac{270}{410} = 0.66. \tag{18}$$

This result is labeled as the analytical result in the figure. However, the viscothermal losses along the walls (partitions) of the chamber provide a slight increase in the total resistance of the chamber. Also, the weak nonlinearity of the wire mesh is not included in the current model.

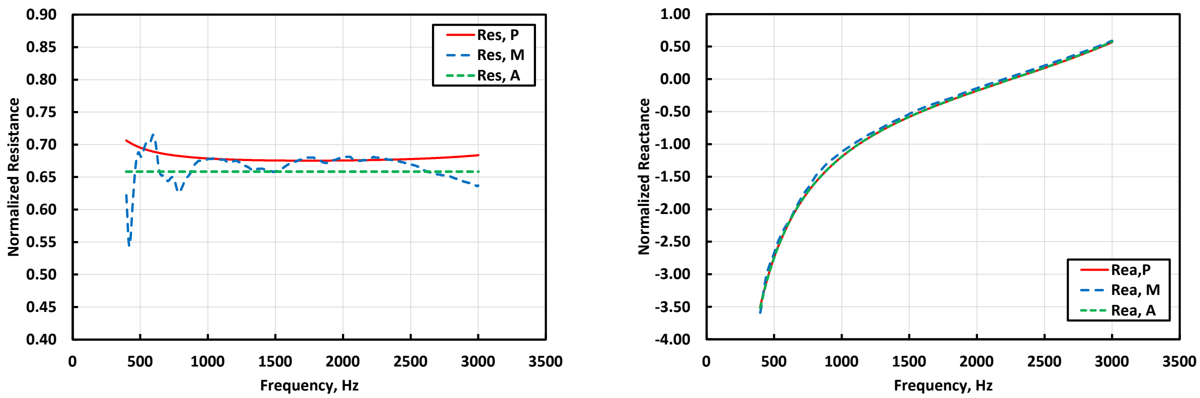

(a) Normalized resistance spectra.

(b) Normalized reactance spectra.

Figure 15: Predicted (P; ZKTL-SC), measured (M), and analytical (A; Eq. [18]) impedance spectra for a mesh over an air gap with a rigid backplate.

The measured resistance spectrum is between the predicted (ZKTL-SC) and analytical (Eq. [18]) values over the majority of the frequency range, with a total spread on the order of 0.02. As expected, the reactance is dominated by contributions due to the air gap. Due to the scale of the reactance plot, small deviations between the respective results are only slightly evident.

5.4 Thin Perforated Layer

Figure 16 provides results for a conventional perforated sheet mounted over a 1.5"-thick air gap with a rigid backplate. This sample was considered in a recent perforate facesheet impedance prediction model study [1], and was selected because it has an open area ratio (0.091) that is close to the center of the typical range used in commercial aircraft. The perforated sheet has holes with a diameter of 0.068" and a sheet thickness of 0.041". A sound pressure level of 120 dB was used for this evaluation.

The prediction captures the general trend of the measured resistance spectrum, but differences remain (note the expanded scale). The predicted resistance increases at resonance (the frequency where the reactance crosses zero with a positive slope), which is also seen in the measured result, albeit at a slightly reduced frequency. The difference in the resonance resistance peak between experiment and prediction is due to discrepancies between the reference microphone SPL and actual surface SPL. The prediction model uses the reference microphone SPL as the value at the liner surface. However, in the experiment, the liner surface SPL can be slightly different due to the small distance between the reference microphone and liner surface. This accounts for the frequency shift between prediction and experiment, and it can be accounted for if desired. There is also a seemingly anomalous spike in the measured resistance at approximately 1050 Hz. Note that there is a very small discontinuity in the corresponding measured reactance spectrum at this frequency, which suggests this behavior might be due to rattle in the perforated sheet.

Regardless, the differences between the predicted and measured results suggest that further improvements to the perforate facesheet model (Eqs. [12 - 14]) are warranted. For this configuration, the reactance is a combination of the air gap (dominated by quarter-wavelength behavior) and the mass reactance (last term in Eq. [12]). As shown in Fig. 16, the comparison with the measured reactance is very favorable.

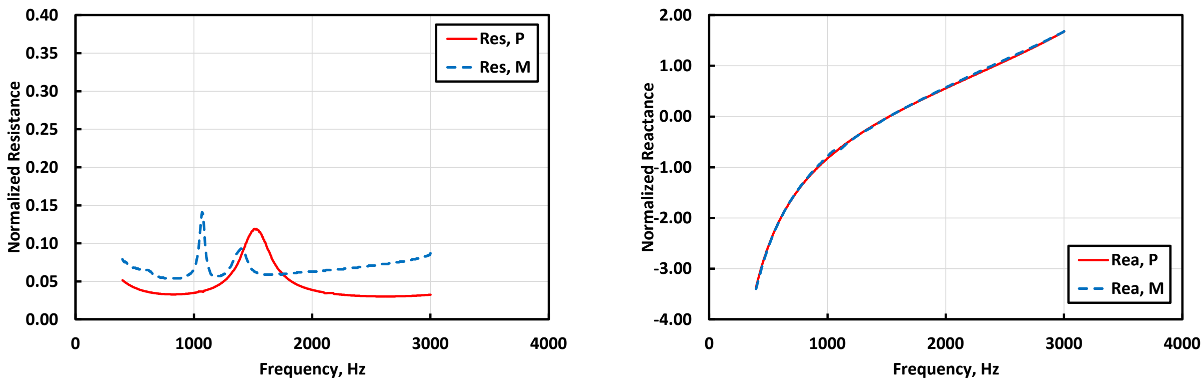

(a) Normalized resistance spectra.

(b) Normalized reactance spectra.

Figure 16: Predicted (P) and measured (M) solutions for a thin perforate over an air gap.

5.5 Thick Perforated Layer

Figure 17 provides results for a thick perforate mounted over a rigid backplate. The 3"×2"×2" perforate has a 19×19 array of 0.05"×0.05" openings. A sound pressure level of 120 dB was used for this prediction and measurement.

The predicted and measured impedance (both resistance and reactance) agree very well for frequencies away from antiresonance. When the impedance magnitude becomes large, the majority of the sound is reflected from the surface. As a result, the liner provides minimal sound absorption. Thus, favorable comparisons between the predicted and measured results are achieved over the frequency range where the liner provides noticeable sound absorption.

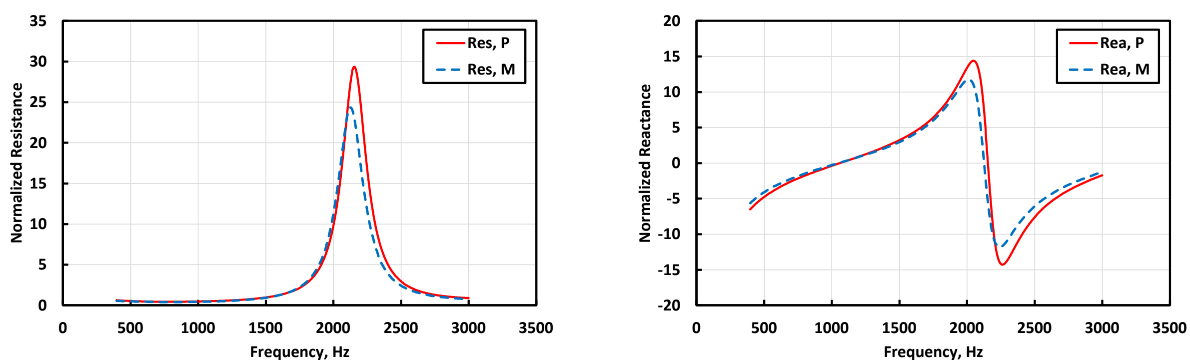

(a) Normalized resistance spectra.

(b) Normalized reactance spectra.

Figure 17: Predicted (P) and measured (M) solutions for a thick perforate over an air gap.

6 Concluding Remarks

This paper presents the latest version of a transmission line model, labeled as ZKTL-SC, used to predict the acoustic impedance at the surface of an acoustic liner. The ZKTL-SC model is comprised of a number of component models used to compute sound transmission through different types of layers that might constitute an acoustic liner. This update incorporates the capability to account for a variety of layer types (including open air, porous material, and perforate layers) that may be combined into a single chamber acoustic impedance prediction by starting at the backplate and ending at the liner surface. The specific acoustic impedance at the surface of this liner chamber is given by the ratio of acoustic pressure to acoustic particle velocity at that location. For uniform liners with sufficiently thin partitions between adjacent chambers, the specific acoustic impedance of the entire liner is equivalent to the impedance of the individual chamber.

If the adjacent chambers have different components, their respective impedances will also differ. A simple approach for computing an equivalent (smeared) impedance over a group of chambers within an acceptable spatial extent (nominally $\lambda/3$ at the highest frequency of interest) was also provided. For those cases where the partitions between adjacent chambers are sufficiently thick, as is often the case for additively-manufactured liners, this updated approach can be used to compute partition effects on the surface impedance.

Comparisons of predicted and measured (or analytical) results were provided for sample cases with each type of liner layer. In general, the comparisons are quite favorable, although there is clearly room for improvement for the modeling of a few of the layer types (the perforate facesheet model in particular). Fortunately, the construction of the transmission line model is such that modifications to any of the individual layer models can be easily incorporated as they become available.

References

1. Jones, M. G., Kreitzman, J. R., and Nark, D. M., "Examination of Perforate Facesheet Impedance Prediction Models," NASA TP 20240006417, Aug. 2024. 1, 3.2.2, 5.4

2. Parrott, T. L. and Jones, M. G., "Parallel-Element Liner Impedances for Improved Absorption of Broadband Sound in Ducts," *Noise Control Engineering Journal*, Vol. 43, No. 6, Nov. 1995. 1

3. Jones, M. G., Watson, W. R., Nark, D. M., Schiller, N. H., and Born, J. C., "Optimization of Variable-Depth Liner Configurations for Increased Broadband Noise Reduction," AIAA Paper 2016-2783, May 2016. 2

4. Jones, M. G. and Nark, D. M., "Partition Thickness Considerations for Additively Manufactured Acoustic Liners," NASA TM 20230013028, Oct. 2023. 2.2.3

5. Motsinger, R. E. and Kraft, R. E., "Design and Performance of Duct Acoustic Treatment: Aeroacoustics of Flight Vehicles; Chapter 14, Vol. 2: Noise Control," NASA RP 1258, Aug. 1991. 2.2.3

6. Zwikker, C. and Kosten, C., *Sound Absorbing Materials*, Elsevier Publishing Company, 1949. 3.1

7. Tijdeman, H., "On the propagation of sound waves in cylindrical tubes," *Journal of Sound and Vibration*, Vol. 39, No. 1, 1975, pp. 1–33. 3.1.1

8. Delany, M. E. and Bazley, E. N., "Acoustical Properties of Fibrous Absorbent Materials," *Applied Acoustics*, Vol. 3, 1970, pp. 105–116. 3.1.2

9. Miki, Y., "Acoustical properties of porous materials-Modifications of Delany-Bazley models-," *Journal of the Acoustical Society of Japan (E)*, Vol. 11, No. 1, 1990, pp. 19–24. 3.1.2

10. Johnson, D. L., Koplik, J., and Dashen, R., "Theory of dynamic permeability and tortuosity in fluid-saturated porous media," *Journal of Fluid Mechanics*, Vol. 176, 1987, pp. 379–402. 3.1.2

11. Champoux, Y. and Allard, J.-F., "Dynamic tortuosity and bulk modulus in air-saturated porous media," *Journal of Applied Physics*, Vol. 70, No. 4, 1991, pp. 1975–1979. 3.1.2

12. Pride, S., Morgan, F., and Gangi, A., "Drag forces of porous-medium acoustics," *Physics Review B*, Vol. 47, No. 9, March 1993, pp. 4964–4978. 3.1.2

13. Lafarge, D., Lemarinier, P., Allard, J. F., and Tarnow, V., "Dynamic compressibility of air in porous structures at audible frequencies," *Journal of the Acoustical Society of America*, Vol. 102, No. 4, Oct. 1997, pp. 1995–2006. 3.1.2

14. Smith, C. D. and Parrott, T. L., "Comparison Of Three Methods For Measuring Acoustic Properties Of Bulk Materials," *Journal of Acoustical Society of America*, Vol. 74, No. 5, 1983, pp. 1577–1582. 3.1.2, 5.2

15. Jones, M. G., Watson, W. R., Nark, D. M., Howerton, B. M., and Brown, M. C., "A Review of Acoustic Liner Experimental Characterization at NASA Langley," NASA TP 220583, April 2020. 3.2.1, 4, 5.2

16. Kreitzman, J. R. and Jones, M. G., "Toward Fully 3D-Printed Two Degree of Freedom Acoustic Liners," AIAA Paper 2024-2801, Jan. 2024. 3.2.2

17. Howerton, B. M., Vold, H., and Jones, M. G., "Application of Sine Sweep Excitation for Acoustic Impedance Eduction," AIAA Paper 2019-2487, May 2019. 4

18. Chung, J. Y. and Blaser, D. A., "Transfer Function Method of Measuring In-Duct Acoustic Properties: I. Theory," *Journal of Acoustical Society of America*, Vol. 68, 1980, pp. 907–921. 4

19. Jones, M. G. and Stiede, P. E., "Comparison of Methods for Determining Specific Acoustic Impedance," *Journal of the Acoustical Society of America*, Vol. 101, No. 5, May 1997, pp. 2694–2704. 4

20. Brown, M. C., Ciletti, A., Godakawela, J., and Sharma, B., "The two-cavity method for characterizing acoustical materials - an interlaboratory study," Noise-Con 2024, June 2024. 5.2